MAPPING DISPERSION OF URBAN AIR POLLUTION WITH REMOTE SENSING

I.K. Wijeratne[a], W. Bijker[b]

[a] Urban Development Authority, GIS Centre, 7th floor, "Sethsiripaya", Battaramulla, Sri Lanka - wijeratne@alumni.itc.nl
[b] International Institute for Geo-information Science and Earth Observation - ITC; P.O. Box 6;
7500AA Enschede, The Netherlands - bijker@itc.nl

KEY WORDS: Urban, Pollution, Mapping, Environment, Temperature, Optical, Landsat

ABSTRACT:

Dispersion of air pollution depends upon various factors including weather conditions, topography and local situation, causing large variation, even in small areas. In addition to mathematical dispersion models and interpolation methods, remote sensing can improve mapping of the spatial distribution of urban air pollution, although no dedicated sensors exist. We used aerosol optical thickness, indicating how much radiance is disturbed on its way through the atmosphere, and at-satellite temperature, calculated from the visible, near infrared and thermal infrared bands of Landsat 7-ETM+. Dispersion of urban air pollution was mapped via a relation between ground station data and aerosol optical thickness and at-satellite temperature. Aerosol optical thickness in green and red bands and at-satellite temperature in thermal infrared band show significant relation with particulate matter, black particles and carbon monoxide respectively. We conclude that spatial variability of these pollutants can be mapped with remote sensing.

1. INTRODUCTION

Air pollution is a major problem in developed and developing countries. It causes respiratory diseases and chronic illness (McCubbin and Delucchi, 1999) and affects soils (El Desouky et al., 1998) and forests (Zhang et al., 2000). Both human activities and natural environmental processes are sources of air pollution. Seasonal changes (Cheng and Lam, 1997) and chemical reactions contribute to the concentration of the polluted air. Many factors cause dispersion of air pollution, including weather conditions, humidity, topography and relief of the area, and local conditions, such as ventilation in traffic corridors and presence of buildings. Air pollution consequently shows high spatial variability, even at short distances.

Generally, the amounts of pollutants and the weather conditions are measured at ground stations. Based on these measurements, spatial distribution of air pollution is estimated and visualized using mathematical dispersion models or interpolation methods (Bozyazi, 1998; Chakraborty et al., 1999; Kassteele, 2006). Because of costs, ground data are collected at a limited number of locations (Builtjes et al., 2001; Ung et al., 2001). With high variability at short distances, use of mathematical models and interpolation methods gives an approximate picture only of the distribution of air pollution. In addition, it is difficult to consider all dispersion factors simultaneously. To overcome these problems, remote sensing techniques can be used.

Urban air pollution mostly occurs in the lower troposphere and is less extensively studied using remote sensing, because of limitations of existing sensors. In the ENVISAT satellite, the SCanning Imaging Absorption spectroMeter for Atmospheric CHartograpY (SCIAMACHY) instrument can detect large amounts of polluted air, such as those originating from industrial areas, in small-scale mapping. SCIAMACHY is a follow–up and extended version of the Global Ozone Monitoring Experiment (GOME) on board ERS-2. Sensors for monitoring aerosols are the Advanced Along Track Scanning Radiometer (AATSR) on board Envisat, and its pre-decessors, the Along Track Scanning Radiometers (ATSR-1 and -2), on board ERS-1 and -2 which provide column-integrated data at coarse resolution (Builtjes et al., 2001). Moderate Resolution Imaging Spectroradiometer MODIS and Multi-angle Imaging SpectroRadiometer (MISR) are sensors at Terra satellite used to detect climate change by aerosols (NASA, 2002). All these instruments have low to medium spatial resolution.

Other air pollution research uses aerosol optical thickness to detect air pollution. Aerosols and gasses in the atmosphere disturb the radiance reaching to the sensor by scattering and absorption. This reduces the contrast of the remotely sensed images (Sifakis et al., 1998). Optical thickness indicates the amount of scattering and absorption by particles and gasses. It can be calculated from multi-spectral images with higher resolution, such as Landsat ETM+.

This study focuses on the mapping of dispersion of air pollution using remote sensing techniques and ground station data. The basic method is a radiometric comparison of a satellite image recorded under polluted conditions, with a reference image acquired under less polluted condition. Ground data were used to select a less polluted reference image. In remote sensing, different algorithms are used to estimate aerosol optical thickness, depending on the sensor and the spectral band (Sifakis and Deschamps, 1992; Sifakis et al., 1998; Retalis et al., 1999; Wald and Baleynaud, 1999; Ung et al., 2001). The relation between ground observations and estimates of aerosol optical thickness is described with linear regression providing the the spatial distribution of air pollution.

2. METHODS

The optical thickness of aerosol scattering and the absorption, in visible and thermal parts of the spectrum was evaluated using a combination of two independent methods, namely the "blurring effect" and the "screening effect".

2.1 Blurring effect

In the visible part of the electromagnetic spectrum, scattering of short-wave radiation by airborne particles causes contrast reduction and distortion of spectral response patterns in remotely sensed images. This so called 'blurring effect' can be estimated using the Aerosol Optical Thickness (AOT) (eq. 5), derived from the basic equation of 'apparent reflectance' at satellite (equation 1) (Sifakis and Deschamps, 1992).

$$\rho^* = \rho \frac{T(\theta_s)T(\theta_v)}{1-\rho S} + \rho_a \quad (1)$$

Where ρ^* = apparent reflectance
ρ = intrinsic surface reflectance
ρ_a = atmospheric or sky reflectance
S = spherical albedo of the atmosphere, defined as a ratio of scattering to total attenuation radiation (i.e. scattering + absorbed)
θ_s = solar zenithal angle
θ_v = observation zenithal angle
$T(\theta_s)$ = total transmission function on the downwelling path, analysed as the sum of $t_{dir}(\theta_s)$ and $t_{diff}(\theta_s)$ which are direct and diffused transmission functions.
$T(\theta_v)$ = total transmission function on the upwelling path, analysed as the sum of $t_{dir}(\theta_v)$ and $t_{diff}(\theta_v)$ which are direct and diffused transmission functions

Sifakis and Deschamps (1992) discuss three stages of this equation, according to the target diameter. For large dimensional targets (> 1km), equation 1 was used. Once the diameter is less than 100m, the adjacency effect is introduced as in equation 2 below. It was assumed that "the standard deviation expresses the analogical contrast in images". Only the first term of equation 2 was used assuming uniform background contribution to all the surrounding pixels. Then the relationship between the standard deviation of apparent reflectance $\sigma(\rho^*)$ and the standard deviation of real reflectance $\sigma(\rho)$ is derived according to equation 3. Another reason to select equation 3 is because urban areas are composed of small targets.

$$\rho^* = \rho \frac{T(\theta_s)t_{dir}(\theta_v)}{1-\rho_e S} + \rho_e \frac{T(\theta_s)t_{diff}(\theta_v)}{1-\rho_e S} + \rho_a \quad (2)$$

where ρ_e = reflectance from the adjacent objects

$$\sigma(\rho^*) = \sigma(\rho)\frac{T(\theta_s)t_{dir}(\theta_v)}{1-\rho S} \quad (3)$$

where $\sigma(\rho^*)$ and $\sigma(\rho)$ are standard deviation of apparent and surface reflectance respectively.

Using Lambert-Bouguer's transmission law, denoting the viewing angle (observation zenith angle) as θ_v and the AOT as τ the AOT along the path equals $\tau/\cos\theta_v$, and equation 3 becomes

$$\sigma(\rho^*) = \sigma(\rho)\frac{T(\theta_s)\exp(-\tau/\cos\theta_v)}{1-\rho S} \quad (4)$$

Equation 4 can be applied to a reference (clear) day and to a polluted day, so their ratio can be written as equation 5. The factor $T(\theta_s)$ may be taken as constant independently of any temporal variation in AOT, because variation of the two components, $t_{dir}(\theta_s)$ and $t_{diff}(\theta_s)$, cancels out (Sifakis and Deschamps, 1992). When τ increases, $t_{dir}(\theta_s)$ diminishes at the same time as $t_{diff}(\theta_s)$ increases and vice-versa.

$$\frac{\sigma_1(\rho)}{\sigma_2(\rho)} = \exp\left((-\tau_1/\cos\theta_{v1}) + (\tau_2/\cos\theta_{v2})\right) \quad (5)$$

where $\sigma_1(\rho)$ and $\sigma_2(\rho)$ are standard deviation of apparent reflectance for reference and polluted days respectively.

Optical thickness can include scattering effect as well as absorption effect due to molecules and particles. This can be written as

$$\tau = \tau_m^a + \tau_p^a + \tau_m^s + \tau_p^s \quad (6)$$

where τ represent optical thickness, superscripts 'a' and 's' represent absorption and scattering, respectively and subscripts 'm' and 'p' represent molecules and particles, respectively.

Absorption due to molecules is minimal in remotely sensed images because sensors use atmospheric windows. For small wavelengths, absorption by particles is negligible and to a lesser degree also in the near-infrared. This is true when the aerosols contain no or few black particles. Rayleigh scattering is caused by gasses (molecules) and can be considered constant in similar atmospheric pressure conditions. Mie scattering is caused by particles with a size around 0.08 to 2.5 μm. With much bigger particles, non-selective scattering can be expected. (Sifakis and Deschamps, 1992). Considering these factors, for small wavelengths, optical thickness calculated using equation 5 can be considered due to particle scattering.

2.2 Screening effect

The screening effect is caused by radiation attenuation of particles, predominantly through absorption, and results in a veiling of the images at longer wavelengths (Sifakis et al., 1998). This effect was estimated with the at-satellite temperature (AT) based on thermal infrared bands with equation 7, using two images. Subscripts 1 and 2 represent the images for reference and polluted days respectively.

$$\Delta T^* = T_1^* - T_2^* = Te_1 - Te_2 + \Delta Ta_1 - \Delta Ta_2 + \Delta Tg_1 - \Delta Tg_2 \quad (7)$$

where T_1^*, T_2^* = observed radiative temperatures measured in the image
Te_1, Te_2 = target's radiative temperatures at the moment of image acquisition
ΔTa_1, ΔTa_2 = local variations of the radiative temperature introduced by the presence of aerosols
ΔTg_1, ΔTg_2 = variations of the radiative temperature due to changes in gas concentration

If there is no noticeable difference in atmospheric pressure between the two days on which the images are taken, then $Tg_1 = Tg_2$. Intrinsic radiative temperature of the targets (Te_1 and Te_2) is subject to variation in solar angle and air temperature. Assuming that (Te_1-Te_2) is constant throughout the land area covered by the scene, however, any remaining decrease in the observed radiative temperature (at-satellite temperature) at pixel level can be attributed to attenuation caused by aerosols (Sifakis et al., 1998).

2.3 Selecting a Grid

The standard deviation of apparent reflectance is calculated on a grid basis. For this study we used a cell corresponding to 600 x 600 m^2 on the ground. According to Sifakis and Deschamps (1992) and Sifakis et al. (1998), grid cell size should be selected in such a way that: a) it is large enough to include some visible ground structure, or, in other words, the spectral response of the ground is assumed to be variable in space but not in time; and b) it is sufficiently small to consider the atmosphere within a grid cell as homogeneous, so variable in time but not in space, hence $\sigma(\rho)$ will be attributed to ground spectral variations exclusively.

Definition of the grid has a large influence on the regression results. We tested two grid types: 'arbitrary grid' with the ground location situated wherever inside the particular grid cell and 'ideal grid', with the ground location situated in the centre of the relevant grid cell, both with the same cell size. For the regression analysis, grid cell values of AOT and AT corresponding to the location of the ground data collection station are considered.

2.4 Regression analysis and mapping

Using linear regression, we established relations between processed image outputs (AOT and AT) and ground data, considering each measured pollutant separately as dependent variable and AOT and AT as independent variables. 'Bivariate Correlation' in SPSS software was used to check the correlation and scatter plots to identify the relation between two variables. Where scatter plots did not show a linear relation, we converted the variables, to obtain a linear relation, e.g. considering 1/y versus x for hyperbolic; ln(y) versus x for exponential and ln(y) and ln(x) for geometric curves (Lipschutz and Schiller, 1998). Different plots were used to evaluate the regression results. Regression analysis shows the best results under ideal grid situation. Therefore these regression equations are used to map air pollution while AOT and AT are known, for those pollutants where concentration shows a sufficiently strong relation with AOT and AT.

2.5 Study area and data

The Southern part of the Netherlands was selected as study area, because it includes both major urban centers like Rotterdam and Utrecht, and rural areas. Suitable ground data and imagery were available for this area. The National Institute of Public Health and the Environment of the Netherlands (Rijksinstituut voor Volksgezondheid en Milieu – RIVM) collects data on an hourly basis for particulate matter (PM10), carbon monoxide (CO), nitrogen monoxide (NO), nitrogen dioxide (NO_2), sulphur dioxide (SO_2), ammonia (NH_3), ozone (O_3) and daily average of black particles (BP), which are available via their website http://www.lml.rivm.nl/. We used data from January 2000 to March 2002. See van Elzakker (2001) for instruments and calibration used in the Dutch air quality network. Figure 1 shows the location of the 28 ground stations in the study area.

Since the method is based on comparison, two remote sensing images in the visible and thermal part of the spectrum were required, one on a clear (less polluted) day and one on a polluted day. Based on the ground data, out of available, cloud-free images of the study area, the Landsat ETM+ image of December 23, 2000 was selected as the image of a polluted day and that of July 3, 2001 as the image of a (relatively) clear day.

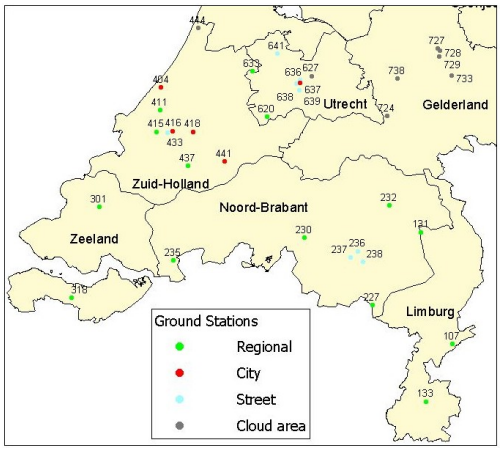

Figure 1. Location of ground stations

3. RESULTS

Figure 2 shows the AOT for bands one to four and AT for band 6. Minimum and maximum values of AOT and AT are given below the relevant figure.

3.1 Regression analysis and mapping

Pixels with clouds and water bodies were excluded from analysis, because correct results are only obtained on land area (Sifakis and Deschamps 1992; Sifakis et al., 1998). Correlation between ground data and image outputs was better under ideal- than under arbitrary grid situation, except for NO_2. The concentrations of components O_3, NO_2, NO and SO_2 were significantly but weakly correlated with AOT. NH_3 did not show correlation with AOT or AT. NH_3 is measured only on three ground locations in the study area. Best relations were found for PM10, BP and CO. Hourly averages of PM10 and daily averages of BP are significantly correlated with AOT (band 2) and AOT (band 3) respectively. Hourly averages of CO show significant relation with AT of band 6. This resulted in the following equations for mapping:

$$Ha\_CO = -363.1 + 20.0 \cdot AT \quad (8)$$

$$Da\_BP = (0.0195 - 0.0042 \cdot \ln(AOT3))^{-1} \quad (9)$$

$$Ha\_PM10 = 47.7 + 25.3 \cdot AOT2 \quad (10)$$

Here, Ha refers to hourly- and Da to daily average and AOT2 and AOT3 refer to the aerosol optical thickness for band 2 and band 3 respectively. The equations were derived for ideal grid, for mapping arbitrary grid was used. Table 1 shows the summary of the statistics of the regression.

Table 2 shows minimum and maximum concentrations of CO, BP and PM10 over the study area. Histograms of estimated polluting components were used to define the classes in final maps (Figures 3 and 4).

In Figure 4, BP and PM10 show high concentrations in the western part of the study area, possibly due to road traffic, industries in the area and high sea traffic at the North Sea. Hammingh et al. (2002) point out that a considerable amount of pollutants in the Netherlands come from the surrounding countries. This may be the reason for the high concentration of PM10 and BP in the southeast and east of the country. In the case of CO, Figure 3 shows that the highest concentrations are in a northeast-southwest belt and the east border, and also in areas like Rotterdam, Utrecht and Eindhoven. In coarse resolution, CO displays more relation to the urban areas and major road network.

To generalize the seasonal effect on AT, the temperature difference of 18.2^0 is considered as lowest in the study area. In other words, if at-satellite temperature difference is higher than 18.2^0 the area is considered polluted with CO. This is almost the same as the difference of air temperature between reference and polluted days in the study area.

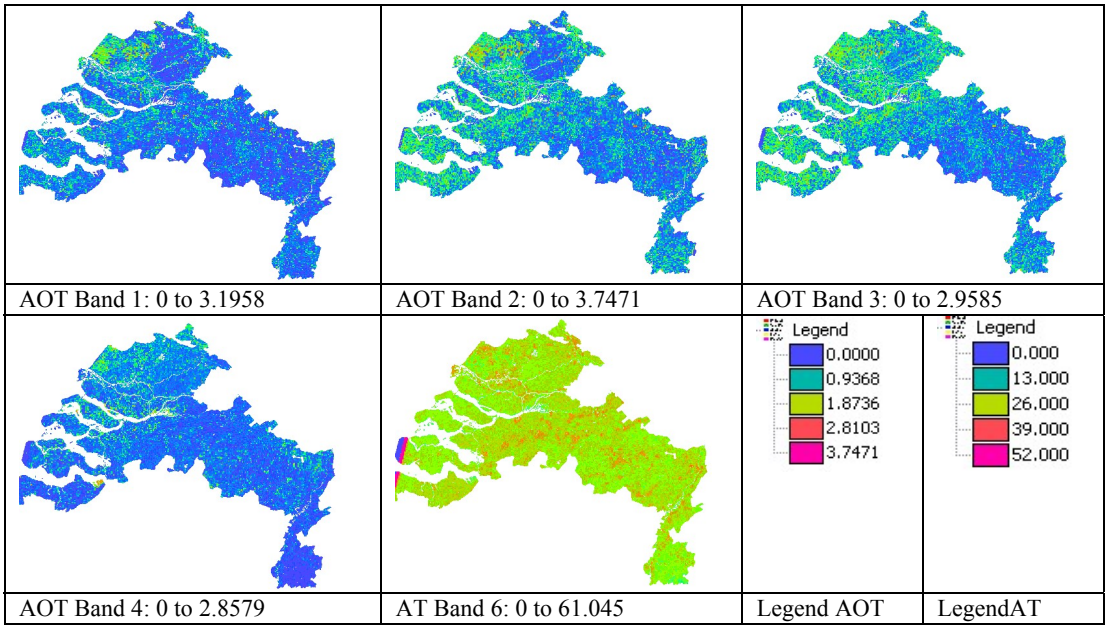

Figure 2. AOT for bands one to four and AT for band 6 of Landsat ETM+, with minimum and maximum values

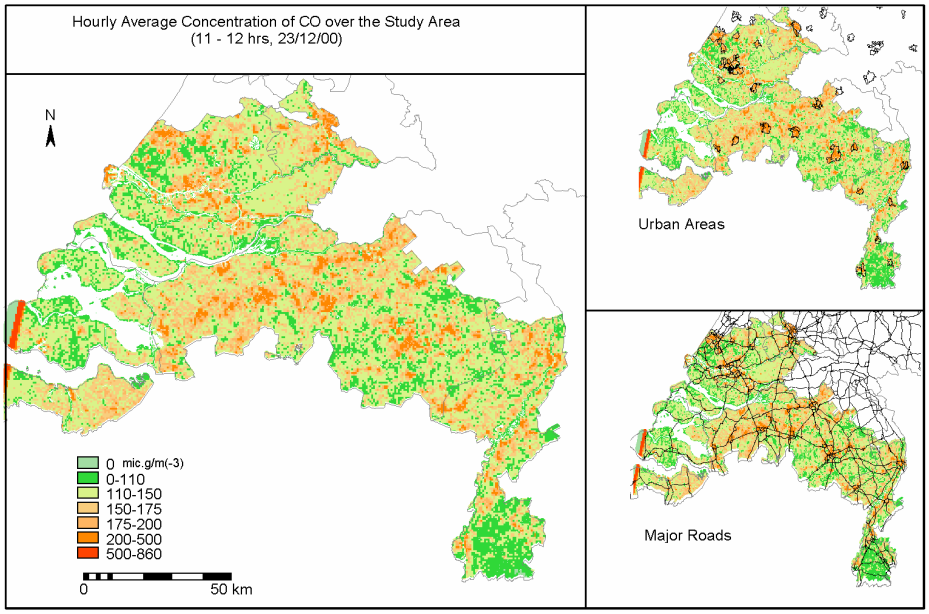

Figure 3. Concentration of CO over the Study Area

Variables	No of cases	Adj. R^2	F	MSE
Ha_CO, AT	13	.53	14.64	36.72
Da_BP, ln(AOT3)	9	.42	6.74	0.005206
Ha_PM10, AOT2	10	.55	11.84	8.89

Table 1. Summary of the statistics of the regression for hourly averages of CO (Ha_CO) and PM10 (Ha_PM10), and daily averages of BP (Da_BP)

	Minimum	Maximum
Black Particles	5.85	66.80
PM10	47.73	142.44
CO	0	856.56

Table 2. Concentration range of BP, PM10 and CO over the Study Area ($\mu g/m^3$)

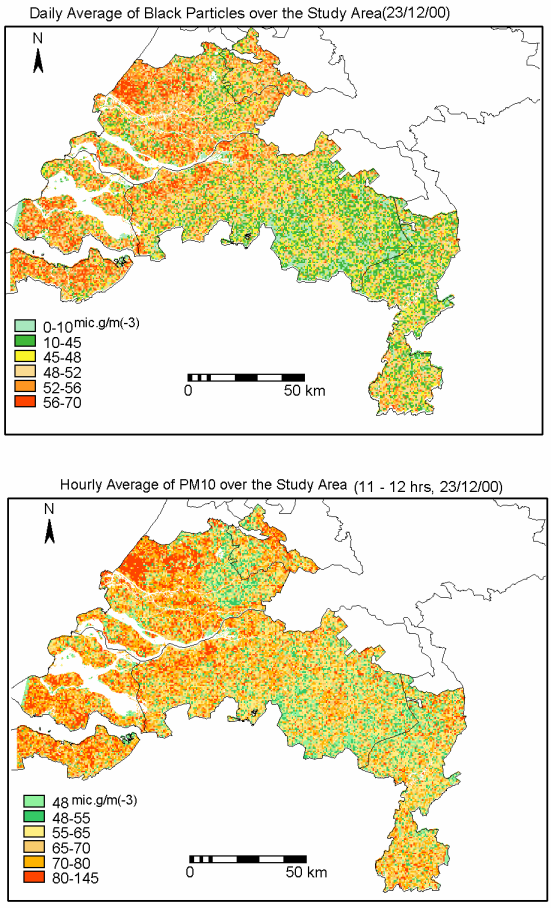

Figure 4: Concentration of Black Particles and Particulate matter over the study area

4. DISCUSSION

PM10 is significantly correlated with AOT2, BP with AOT3 and CO with AT. NO_2 is correlated with AOT3 and AT, NO and O_3 with AOT3, and SO_2 with AOT2. Particle size of aerosols generated by pollutants may be a reason for the fact that different components have relations with AOT or AT of different bands. Another reason may be their chemical and physical properties.

Selecting a reference and a polluted day is very important in this kind of study. One possibility to do this is to check the pollution level from the ground data, for the recording date of the available images. Another possibility is checking the histograms of DN values of visible bands. For polluted days shrinkage of histograms with a low standard deviation can be expected. To do a histogram check, there should be an image archive.

Ideal grids, with the ground observation in the centre of a grid cell gave better results for regression analysis than arbitrary grids, where ground observations close to the border of a cell are a source of error. Therefore accuracy of georeferencing and of ground-station coordinates are also important.

To check the effect of cell size on the results, a 450 x 450 m^2 ideal grid was tested. When grid cell size is changed, temperature differences do not change significantly, because AT is calculated as the average of the pixels in the considered grid cell. In the case of AOT, the effect of a smaller cell size can be positive or negative, possibly because AOT is based on the standard deviation of the selected grid cell. If the area's texture changes rapidly, then changing grid cell size affects AOT.

If the area has high deposition rate, the measurements at ground level show higher pollutant values than the image outputs. In other areas, values from measurements at ground level are much lower than estimates from images. A possible explanation is that pollution form a local source is released to the atmosphere and spreads over the area, but not at ground level.

As can be seen from equation 8, at satellite temperature difference should be at least 18.2° to estimate presence of CO. Air temperature difference between reference and polluted day is more than 18.2° over almost the entire study area, only an area of 14.6 km^2 (0.13%) does not reach this threshold. When calculating at-satellite temperature (screening effect), using equation 8 it is assumed that the 'target radiative temperature' is constant. Sifakis et al. (1998) explain that this depends on variation in solar angle and air temperature. To generalize the seasonal effect and to remove the effect by target radiative temperature, 18.2° was used as a cutoff value in this study. So, if the at-satellite temperature difference is higher than 18.2°, the area is considered polluted with CO.

Equations 8, 9 and 10 can be used to estimate the concentration of hourly average of CO, PM10 and daily average of BP for any part of the study area, once the AOT or AT are known from images, per cell of 600 x 600 m^2. For other grid cell sizes new calibration is needed. Other image pairs will need another temperature cut-off value, depending on the seasonal difference. New sources of air pollution with other components having a scattering or absorption effect will also require recalibration of the equations.

5. CONCLUSIONS

Hourly averages of CO and PM10 and daily averages of BP show a good relation with their estimates calculated from images via AT (band 6), AOT (band 2) and AOT (band 3) respectively. At some locations, however, values from ground measurements are much lower than the estimates from images. In such situation pollution can be detected by remotely sensed images, but not by ground level data. If the area has high

deposition rate, the pollutant collected at ground level shows a higher value than the image outputs.
Geo-referencing and removing water bodies and cloud cover are important. For a regression analysis between ground data and aerosol optical thickness from images, it gives the best result, when the ground station is situated in the centre of the corresponding grid cells of the image(s). For most of the urban areas 600 by 600 m^2 grid cell size is suitable. Checking the suitable grid cell size for the study area is important because it has an effect on the regression results.

This study shows how remote sensing can be used to map the spatial variability of urban air pollution by CO, PM10 and BP. The greater spatial detail provided can be used to improve estimates based on interpolation between ground observations and dispersion models.

REFERENCES

Bozyazi, E.G., 1998. *Analysis and Mapping of Air Pollution: A GIS Approach: A case study of Istanbul, Turkey.* International Institute for Aerospace Survey and Earth Sciences (ITC), Enschede, The Netherlands. MSc thesis.

Builtjes, P.J.H., H.M ten Brink, G. de Leeuw, M. van Loon, C. Robles González, M. Schaap, 2001. *Aerosol air quality satellite data - Final report*. USP-2 report 00-33. Beleids Commissie Remote Sensing, Delft, The Netherlands.

Chakraborty, J., L.A. Schweitzer, D.J. Forkenbrock, 1999. Using GIS to assess the environmental justice consequences of transportation system changes. *Transactions in GIS*, 3(3), pp. 239 - 258.

Cheng, S. and K.C. Lam, 1997. Climatic Impact on air pollution concentrations in Hong Kong. Department of Geography, Occasional paper, The Chinese University of Hong Kong, Hong Kong.

El Desouky, H.J., K.F. Moussa and H.H. Hassona, 1998. Impact of automobile exhaust on roadside-soils and plants in Sharkiya Governorate. *Egyptian Journal of Soil Science* 38(1-4), pp. 137-151.

Elzakker, B. G. van, 2001. *Monitoring activities in the Dutch National Air Quality Monitoring Network in 2000 and 2001*. RIVM Report 723101 055. National Institute of Public Health and the Environment RIVM, Bilthoven, The Netherlands.

Hammingh, P. (ed.), J. Beck, P. van Breugel, E. Buijsman, H. Diederen, E. Noordijk, J. de Ruiter, J. Tromp, G. Velders, K van Velze, 2002. *Jaaroverzicht luchtkwaliteit 2001*. RIVM rapport 75301009, RIVM, Bilthoven, The Netherlands.

Kassteele, J. van de, 2006. *Statistical air quality mapping*. Doctoral thesis Wageningen University, Wageningen, The Netherlands.

Lipschutz, S. and J. Schiller, 1998. *Schaum's Outline of Theory and Problems of Introduction to Probability and Statistics.* McGraw Hill, New York, etc.

McCubbin, D. R. and M. A. Delucchi, 1999. The health costs of motor vehicle related air pollution. *Journal of Transport Economics and Policy* 33(3), pp. 253 - 286.

NASA, 2002. Landsat 7 Science Data Users Handbook, Chapter 11 Data Products. http://ltpwww.gsfc.nasa.gov/IAS/handbook/handbook_htmls/chapter11/chapter11.html

Retalis, A., C. Cartalis and E. Athanassiou, 1999. Assessment of the distribution of aerosols in the Athens with the use of Landsat Thematic Mapper data. *International Journal of Remote Sensing*, 20(5), pp 939 - 945.

RIVM- National Institute of Public health and the Environment of the Netherlands/Rijksinstituut voor Volksgezondheid en Milieu http://www.lml.rivm.nl/.

Sifakis, N. and P. Y. Deschamps, 1992. Mapping of air pollution using SPOT satellite data. *Photogrammetric Engineering and Remote Sensing* LVIII, pp. 1433 - 1437.

Sifakis, N., N.A. Soulakellis and D. Paronis, 1998. Quantitative mapping of air pollution density using Earth observations: A new processing method and application on an urban area. *International Journal of Remote Sensing* 19(17), pp. 3289 - 3300.

Ung, A., Wald, L. and Ranchin, T., 2001. *Satellite data for air pollution mapping over a city Virtual stations. In: Proceedings of the 21th EARSeL Symposium, Observing our environment from space: new solutions for a new millennium, Paris, France, 14-16 may 2001.* ed by Gérard Begni. Lisse, etc. A. A. Balkema. pp. 147-151.

Wald, L. and J. M. Baleynaud, 1999. Observed air quality over city of Nantes by means of Landsat themal infrared data. *International Journal of Remote Sensing* 20(5), pp. 947 - 959.

Zhang Jin Tun, R. Pouyat, J.T. Zhang (2000). Effects of urbanization on the concentrations of heavy metals in deciduous forest floor in a case study of New York City. *Scientia Silvae Sinicae* 36(4), pp. 42 - 45.

ACKNOWLEDGEMENTS

We thank the Netherlands' Fellowship Programme for providing the funds for the study, the National Institute of Public Health and Environment of the Netherlands (RIVM) for their data and reports and professor A. Stein (ITC) for his helpful comments.